PNAS

Supporting Information for

Comparative connectomics reveals non-canonical wiring for color vision in human foveal retina.

Yeon Jin Kim, Orin Packer, Andreas Pollreisz, Paul R. Martin, Ulrike Grünert, and Dennis M. Dacey*

*Corresponding author: Dennis M. Dacey
Email: dmd@uw.edu

This PDF file includes:

Supporting Information Text

Materials and Methods

Serial block-face SEM sample preparation and image acquisition

Tissue acquisition: Human eyes (52-year-old, white male; brain dead organ donor) were acquired at time of death by surgical enucleation from the Medical University of Vienna, Vienna, Austria. The eyes were immersion fixed for electron microscopy in 4% glutaraldehyde in 0.1M sodium cacodylate buffer, pH7.3-7.4 for 30 minutes to 1 hour at room temperature. Medical history confirmed no abnormalities of the visual system recorded and no driving limitations; the ocular status was defined medically as unremarkable at time of enucleation. An additional human eye (21 yr old male) acquired by the same method at the University of Washington was also studied (1) and confirmed the results of the present study with regard to S cone connectivity.

A single marmoset eye from an adult 6-year-old male marmoset (*Callithrix jacchus*) was obtained at the end of an unrelated electrophysiological experiment carried out at Monash University in Melbourne, Australia. All procedures were conducted according to the provisions of the NHMRC code of practice for the care and use of animals and were approved by the Monash University Animal Ethics committee that also monitored the welfare of the animals. The animal was overdosed with sodium pentobarbital and then perfused with artificial cerebrospinal fluid. Subsequently, the eyes were removed, and the posterior eyecup was fixed for 2 hours as described above. After rinses in cacodylate buffer, the retina was dissected, cut into smaller pieces which were kept in cacodylate buffer and shipped to The University of Washington.

Pieces of central retina (marmoset: ~300 µm eccentricity, human; ~500 µm eccentricity) were dissected and prepared for EM and ultrathin sectioning in the vertical plane as described previously (2). The tissue block was mounted in a Volumescope SEM (Thermo Fisher) for serial block-face scanning electron microscopy. Regions of interest (ROIs) were defined that encompassed the full depth of the retinal circuitry (~200 x 200 µm ROI divided into 40 x 40 µm tiles) from cone pedicles to the ganglion cell layer. The block faces for both the marmoset and

human sample were sectioned at 50 nm (marmoset, ~1227 sections; human, 1904 sections) and scanned at 5 nm x-y resolution after each section (voxel: 5 x 5 x 50 nm). The resulting set of TIFF images was filtered, contrast normalized, stitched into composite layers and aligned using procedures available with TrakEM2 (NIH Fiji) software. All cell and circuit reconstructions were also performed using TrakEM2 to first create arbor skeletons; nodes within these skeletons were used to tag pre- and postsynaptic synaptic structures so that the locations and number of synapses for a given cell could be determined. In selected neurons complete volume rendering was also performed with TrakEM2 painting tools and rendered as 3D mesh objects that could be saved and moved to other programs or viewers for the creation of 2D images.

The focus in this study was the clear identification of ribbon synapses made by cone pedicles and bipolar cell axon terminals. Synaptic ribbons were easily discernable platelike structures, ~25 nm thick and ~250 nm wide and associated with a halo of synaptic vesicles; it was thus easy to identify them unequivocally in our volumes. We used multiple annotators to confirm ground truth skeleton structure, total ribbon numbers and synaptic connectivity during the process of skeletonization and circuit reconstruction.

The preparation of a foveal volume from the retina of a macaque monkey (adult, male, *Macaca nemestrina*) has been described in detail in a previous study of S cone connectivity in this species(25). Here we will just note a few differences from the human and marmoset in how this volume was generated. After tissue fixation, embedding and ROI localization to the foveal slope (~400 µm retinal eccentricity) block-face scanning electron microscopy was performed with a Zeiss/GATAN 3View SEM. The ROI size and location was a close match to that of the marmoset, but fewer and thicker sections (420 sections at 80 nm) were cut during the imaging process. Otherwise, layer alignment, circuit reconstruction, synapse identification was performed using TrakEM2 as described for the human and marmoset samples. The macaque, marmoset and human samples were taken at a point where the foveal slope diminishes, and the ganglion cell layer achieves maximal thickness. Previous measurements of ganglion cell displacement indicate

that ganglion cells at this eccentricity would be linked to cones within 100 μm of the foveal center (3, 4), well within the central 1 degree of the visual field and the region of peak visual acuity.

Principal component analysis and unsupervised classification of S and LM cones

For each S and LM (non-S cone) cone the following parameters were measured: number of ribbons and number of telodendria contacting neighboring cones. Data were analyzed using the functions *pca* (principal component analysis) and *kmeans* (K-means clustering) in Matlab V9.12 (Mathworks, Natick, NJ).

Data availability

All study data are included in the article and/or supporting information.

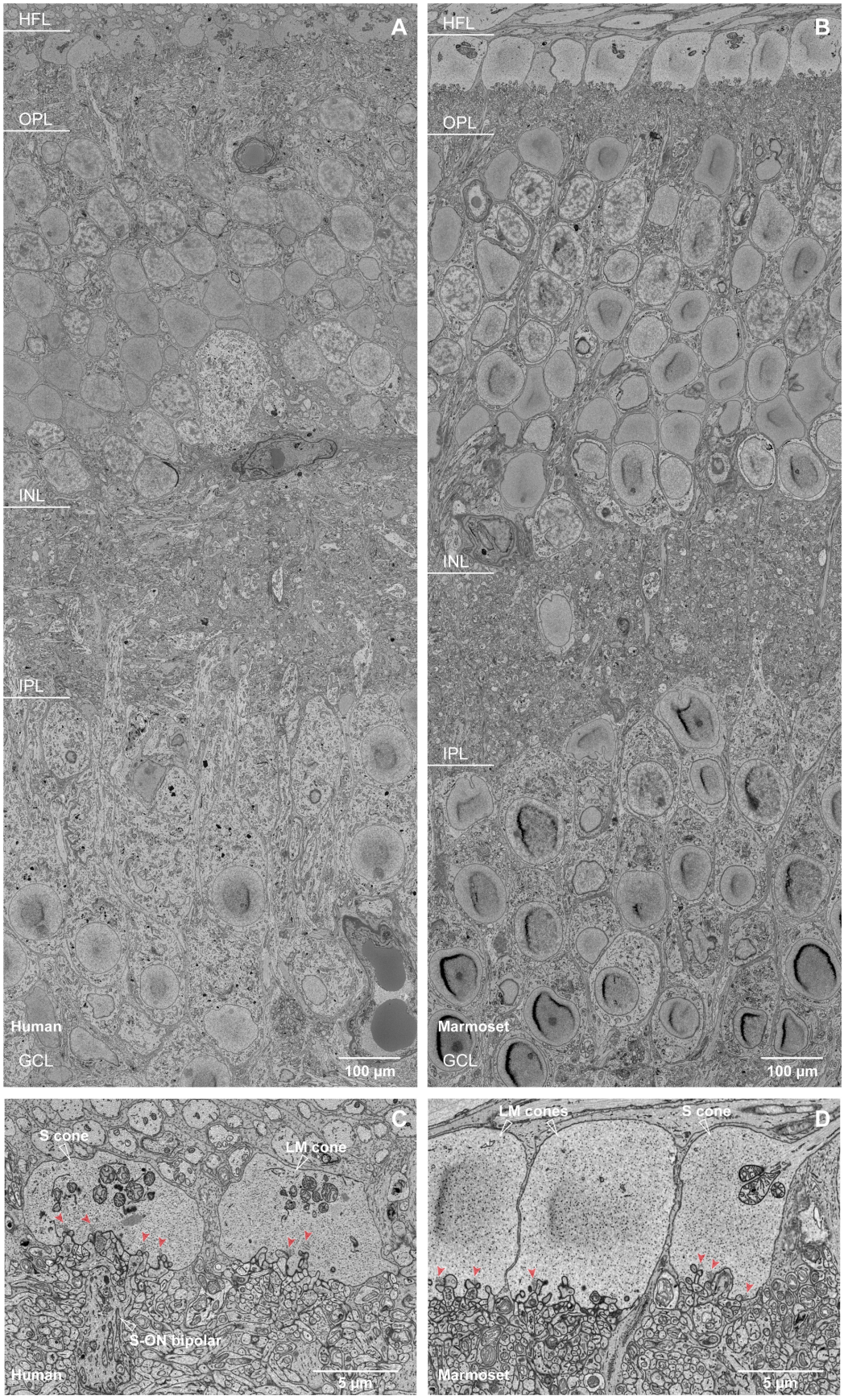
HFL
A
OPL
INL
IPL
Human
GCL
100 µm
HFL
B
OPL
INL
IPL
Marmoset
GCL
100 µm
S cone
C
LM cone
S-ON bipolar
Human
5 µm
LM cones
S cone
D
Marmoset
5 µm

Fig. S1. Human and marmoset volumes are comparable in staining and ultrastructure preservation. A. Example of a single image layer from the human retinal volume (1904 total layers; 50 nm section thickness) sampled at ~500 µm retinal eccentricity (~2 degrees visual angle). Henle fiber layer (HFL) at top and Ganglion Cell Layer at bottom (GCL) of image. At this central eccentricity the GCL is several cell layers thick and extends slightly beyond the bottom of this volume. **B**. Single image layer from the marmoset retinal volume matched in magnification and approximate retinal location (1227 total layers; 50 nm section thickness; ~300 µm retinal eccentricity; at 130 µm/degree, ~2.5 degrees visual angle) to the human retinal volume. HFL, Henle fiber layer; OPL, outer plexiform layer; INL, inner nuclear layer; GCL, ganglion cell layer. **C**. Zoomed image layer of the OPL in the human volume showing Henle fibers at top (cut in cross section), cone pedicles at center and OPL at bottom. Pedicle at the left was identified as an S cone; note the similarity in pedicle morphology to the LM cone on the right. Cone synaptic ribbons are indicated by the red arrowheads; the dendrite of a BB cell beneath the S cone pedicle is indicated. **D**. Zoomed image layer of the OPL in the marmoset volume showing a comparable view to **C**; HFL at top, cone pedicles at center, OPL at bottom. Pedicle at right was identified as an S cone; note its small size relative to the neighboring LM cones. Red arrowheads indicate cone synaptic ribbons.

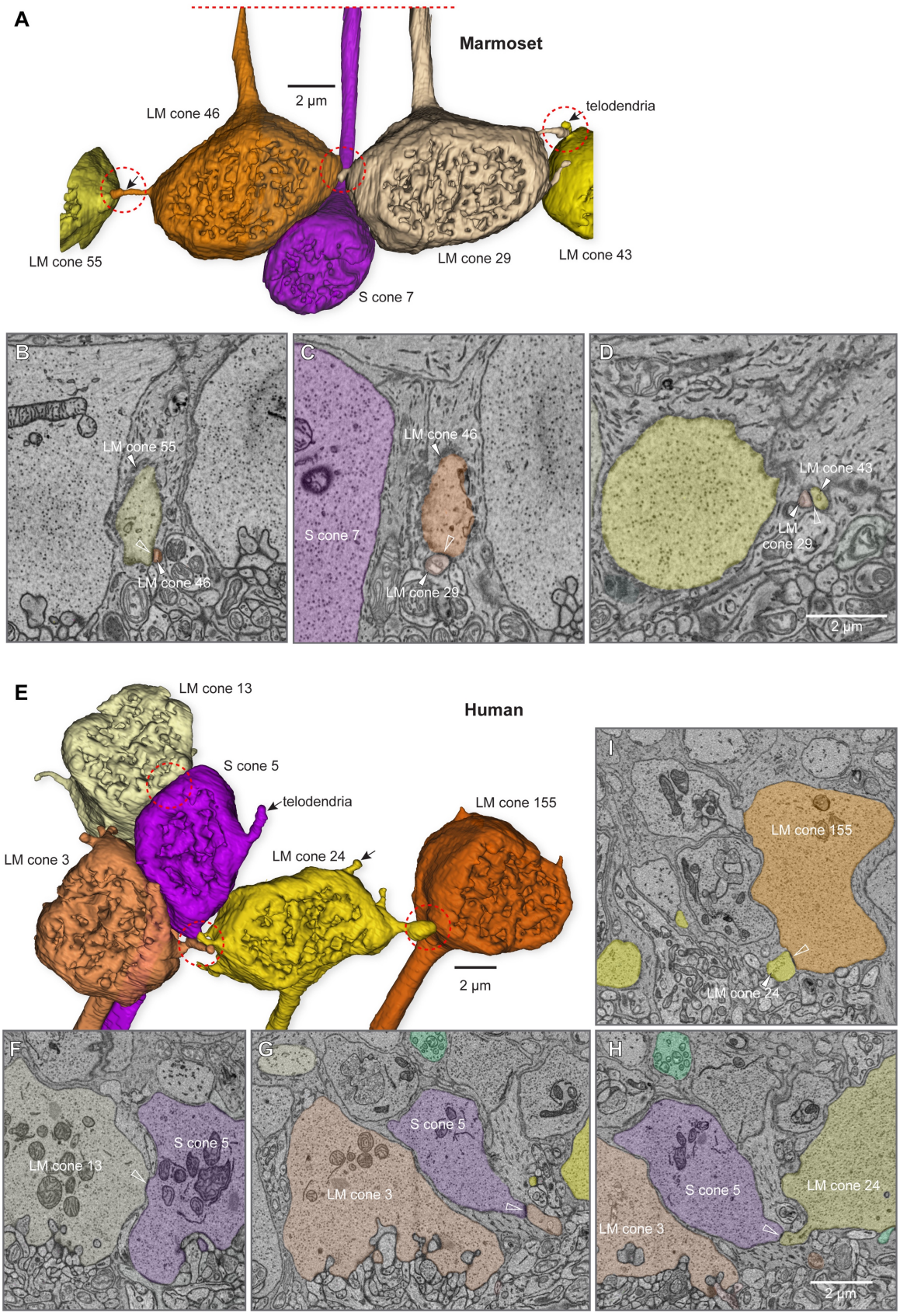
A
Marmoset
2 µm
LM cone 46
telodendria
LM cone 55
LM cone 29
LM cone 43
S cone 7
B
LM cone 55
LM cone 46
C
LM cone 46
S cone 7
LM cone 29
D
LM cone 43
LM cone 29
2 µm
E
LM cone 13
Human
S cone 5
telodendria
LM cone 155
LM cone 3
LM cone 24
2 µm
I
LM cone 155
LM cone 24
F
S cone 5
LM cone 13
G
S cone 5
LM cone 3
H
S cone 5
LM cone 24
LM cone 3
2 µm

Fig. S2. Morphology and pattern of telodendritic contacts between cones in marmoset and human retinas. By contrast with human cone pedicles, the cone pedicles in marmoset give rise to very few telodendria (Marmoset: LM cones: mean ± sd = 2.44 ± 0.97; n = 45; S cones: mean ± sd = 0.00 ± 0.00; n = 9; Human: LM cones: mean ± sd = 8.11 ± 1.85; n = 45; S cones: mean ± sd = 4.12 ± 1.36; n = 17) and also appear very small in diameter compared to their human counterparts. **A**. Total telodendritic contacts for four neighboring LM cones are illustrated in the marmoset retina reconstruction. **B**-**D**. Each panel shows a pair of cones (labeled by number) from the reconstruction in **A** at the point where telodendritic connections occur (points of telodendritic contact marked by the open white arrowhead). **E**. Total telodendritic contacts for single S cone and four neighboring LM cones are illustrated in the human retina reconstruction. **F**-**I**. Each panel shows a pair of cones (labeled by number) from the reconstruction in **E** at the point where telodendritic connections occur. Specifically, S cone 5 makes substantial telodendritic contacts with neighboring LM cone 13 in **F**, LM cone 3 in **G**, and LM cone 24 in **H**. Two neighboring LM cones (LM cone 155 and 24) also make telodendritic contact in **I** (points of telodendritic contact marked by the open white arrowhead).

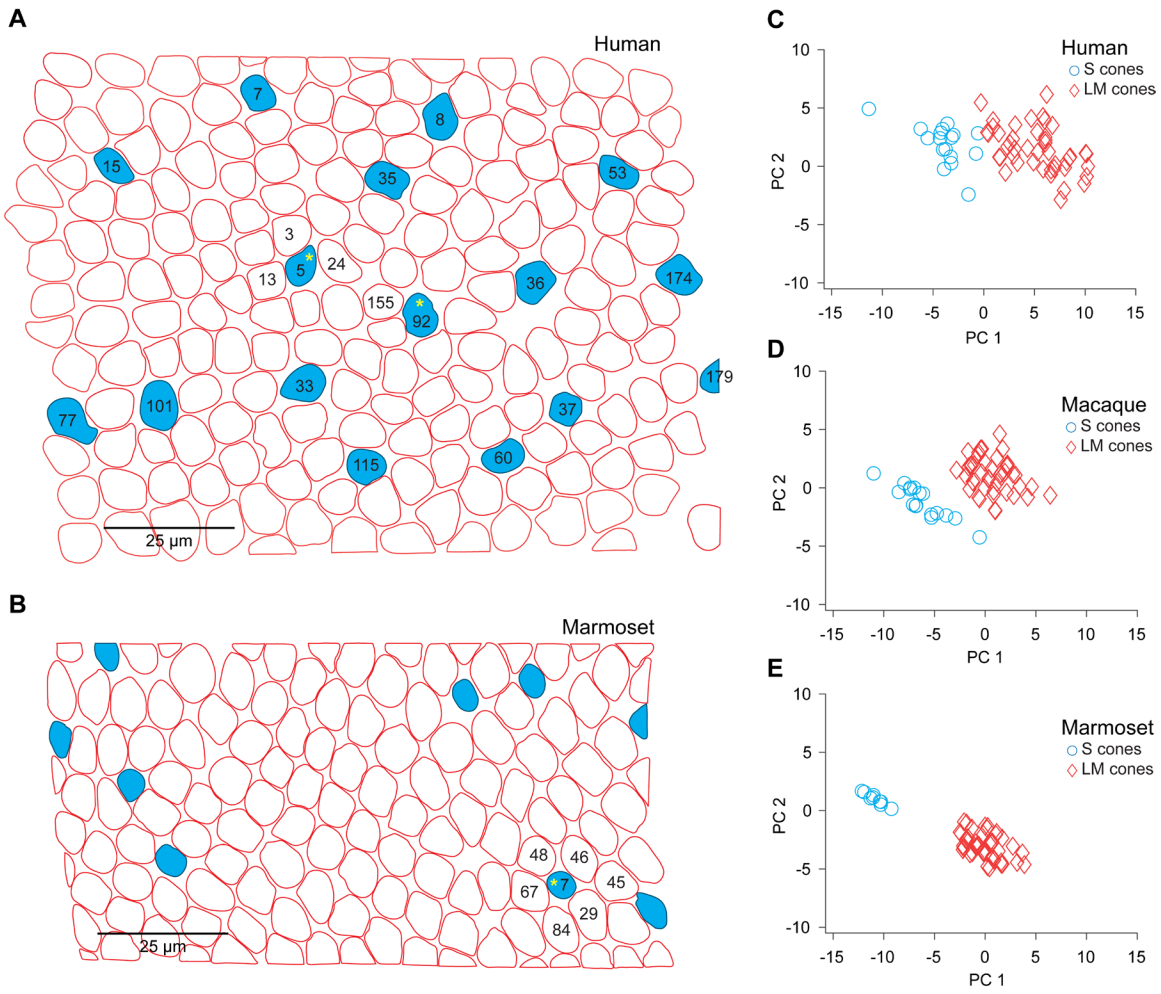

Fig. S3. Mosaics of LM and S cone pedicles in human and marmoset retinal volumes. **A**. Horizontal view of the cone pedicle layer in the human volume. Lines were traced around all cone pedicles at or near their maximum diameters to produce and image of the overall cone mosaic showing the locations of all S cones (blue filled outlines; a total of 17 S cones were identified; 16 complete S cones, one partial S cone on the volume edge; one S cone lies off the main mosaic on the left side and is not shown). Note that the sparse human S cone pedicles are not easily identified by size/diameter relative to surrounding LM cones. The reconstructed S cones (S cones 5 and 92) shown in Fig. 2 are indicated by the yellow asterisks. **B**. Horizontal view of the cone pedicle layer in the total marmoset volume, prepared in the same way as for the human retina and showing the number and location of all identified S cones (blue filled outlines) in the volume (blue filled outlines; a total of 9 S cones were identified; 8 complete and 1 partial S cone at volume edge). The S cone (S cone 7) reconstructed and illustrated in Figs. 1 and 5 and *SI Appendix*, Figs. S3-7 is indicated by the yellow asterisk. **C-E**. Unsupervised cluster Principal components 1 and 2 derived from (for each cone) the number of ribbons, number of telodendria contacting neighboring cones, and number of telodendria contacting neighboring rods. These parameters explained respectively 7%, 18% and 74% of the data set variance. The S and LM

cones occupy distinct clusters in the principal component space derived from simultaneous analysis of the three species, indicating both common and distinct properties of S and LM cones across groups. Consistently, unsupervised K-means clustering yielded congruence with identities based on morphological criteria for all marmoset S and LM cones, and for at least 60% of macaque and human S and LM cones.

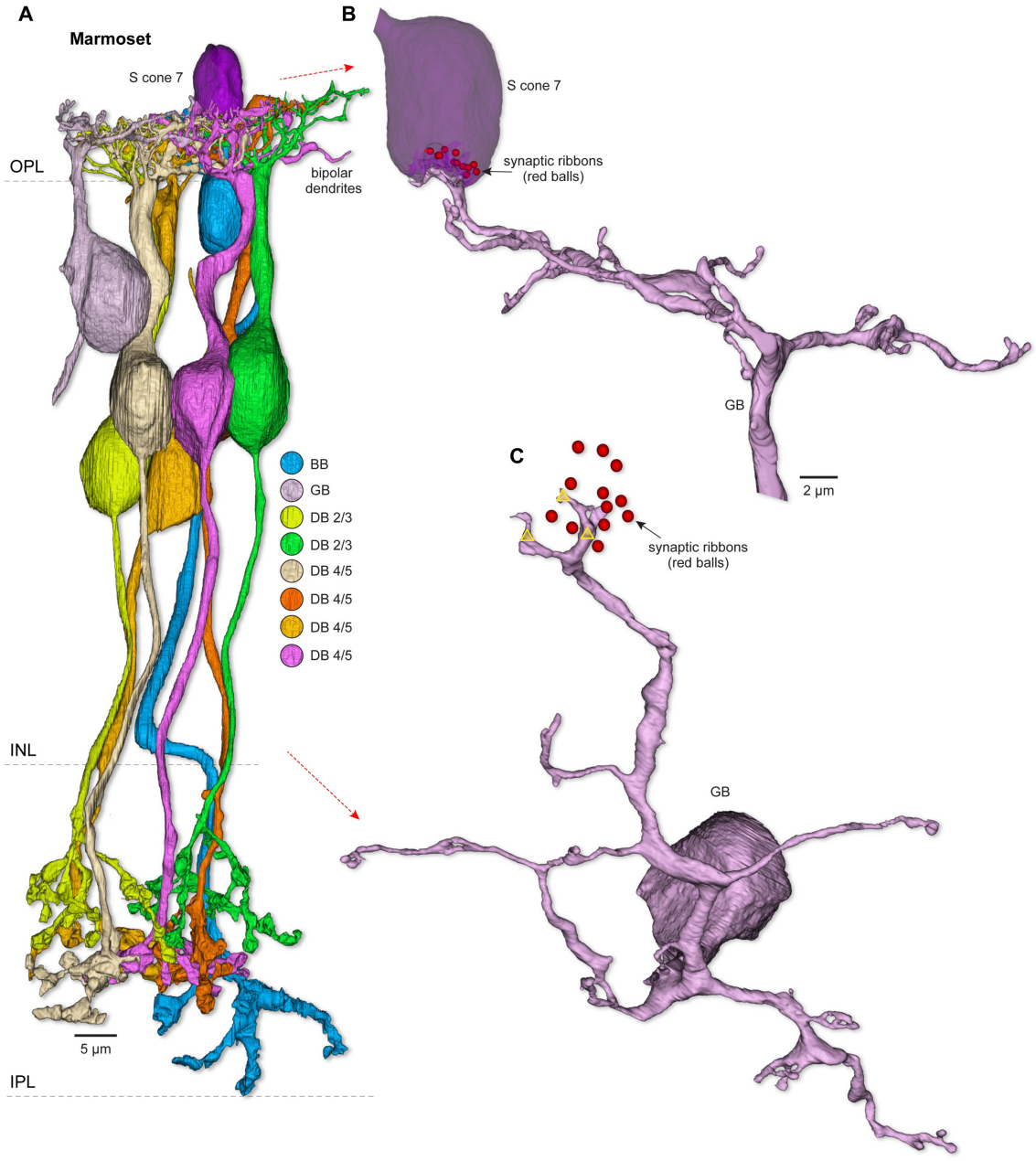

Fig. S4. Identification of the eight bipolar cells postsynaptic to marmoset S cone 7. This and the following *SI Appendix*, Figs. S5-S7 provide a detailed view of each of the diffuse bipolar (DB) cell types making flat contacts with the S cone 7 shown in main Fig. 5. **A**. All DB cells in contact with the S cone 7 are shown in vertical view, showing their relative axonal stratification positions; a single BB bipolar (blue) in contact with this S cone is also shown for reference. Color code identifies three DB types based on axonal stratification and morphology (DB 2/3, yellow and green cells; DB 4/5, gold and violet cells; DB 4/5, tan and orange; Giant bipolar (GB), light violet). **B**. Vertical image view of GB terminal dendritic tree and disposition relative to S cone 7. **C**.

Horizontal image view of GB dendritic tree showing the dendritic tips that made flat contacts with this S cone's synaptic face at 3 locations (indicated by the yellow triangles; the cluster of S cone synaptic ribbons are shown as red balls). This GB cell displays a large dendritic tree relative to other DB types and its dendrites skip over cones contacting widely separated cones sparsely.

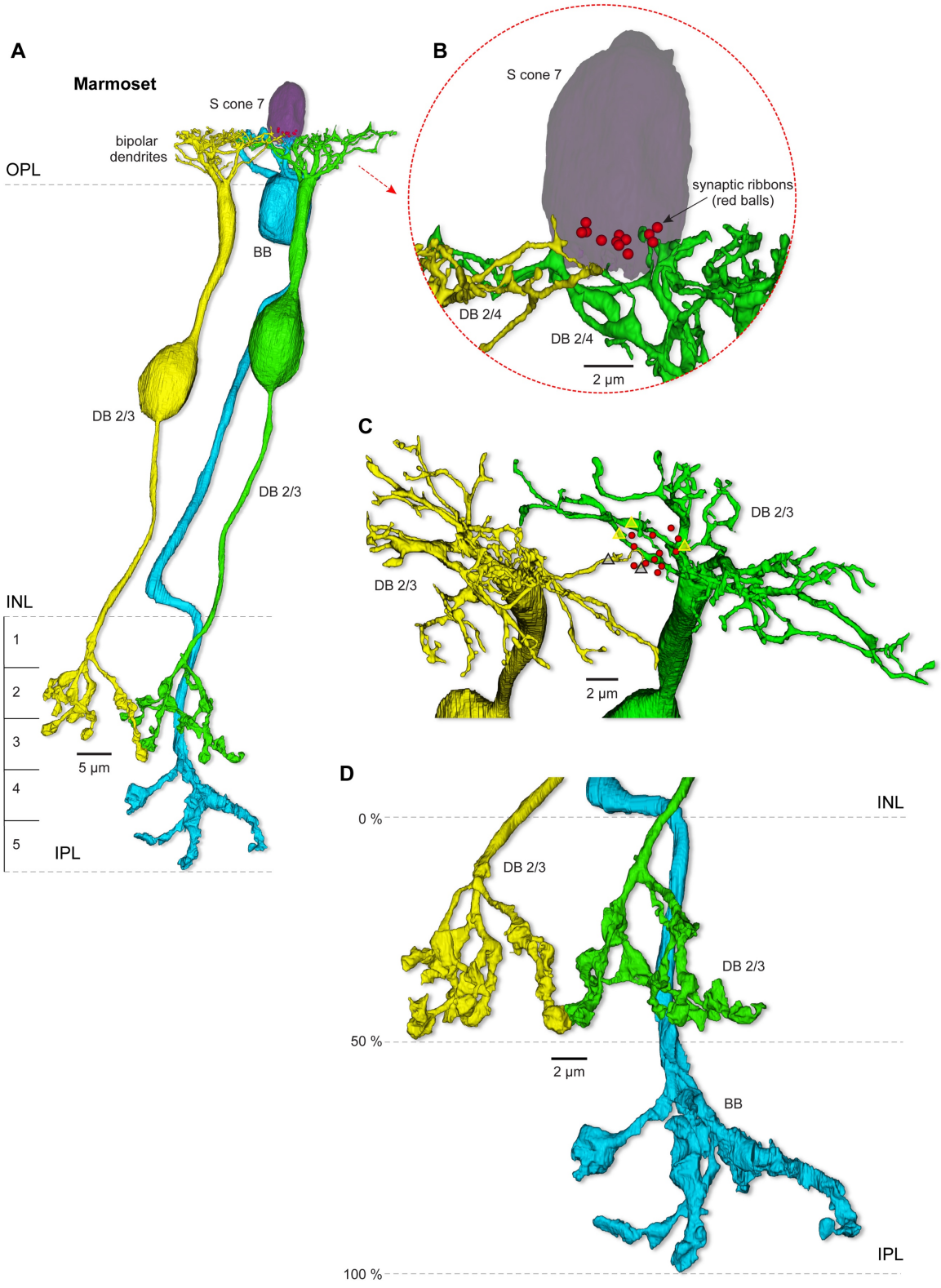

Fig. S5. Identification of two presumed OFF bipolar cells (DB 2/3) postsynaptic to marmoset S cone 7. A. Vertical image view of two proposed DB 2/3 cells (yellow and green)

postsynaptic to S cone 7, shows both dendritic trees and axon terminals in relation to one of three BB cells targeting this S cone. **B**. Zoomed view of neighboring DB 2/3 cells making flat contact with S cone 7. **C**. Dendritic trees of the two proposed DB 2/3 cells tile the space around S cone 7 (5 synaptic contacts with the pedicle face are indicated by the yellow and black triangles; the cluster of S cone synaptic ribbons are shown as red balls) with little dendritic overlap. Note that all DB cells receive their major input from LM cones as indicated by the many dendritic terminals surrounding this S cone. **D**. Zoomed view of axon terminal stratification in the IPL; these two neighboring cells showed identical stratification depth in the outer IPL (20-50% depth).

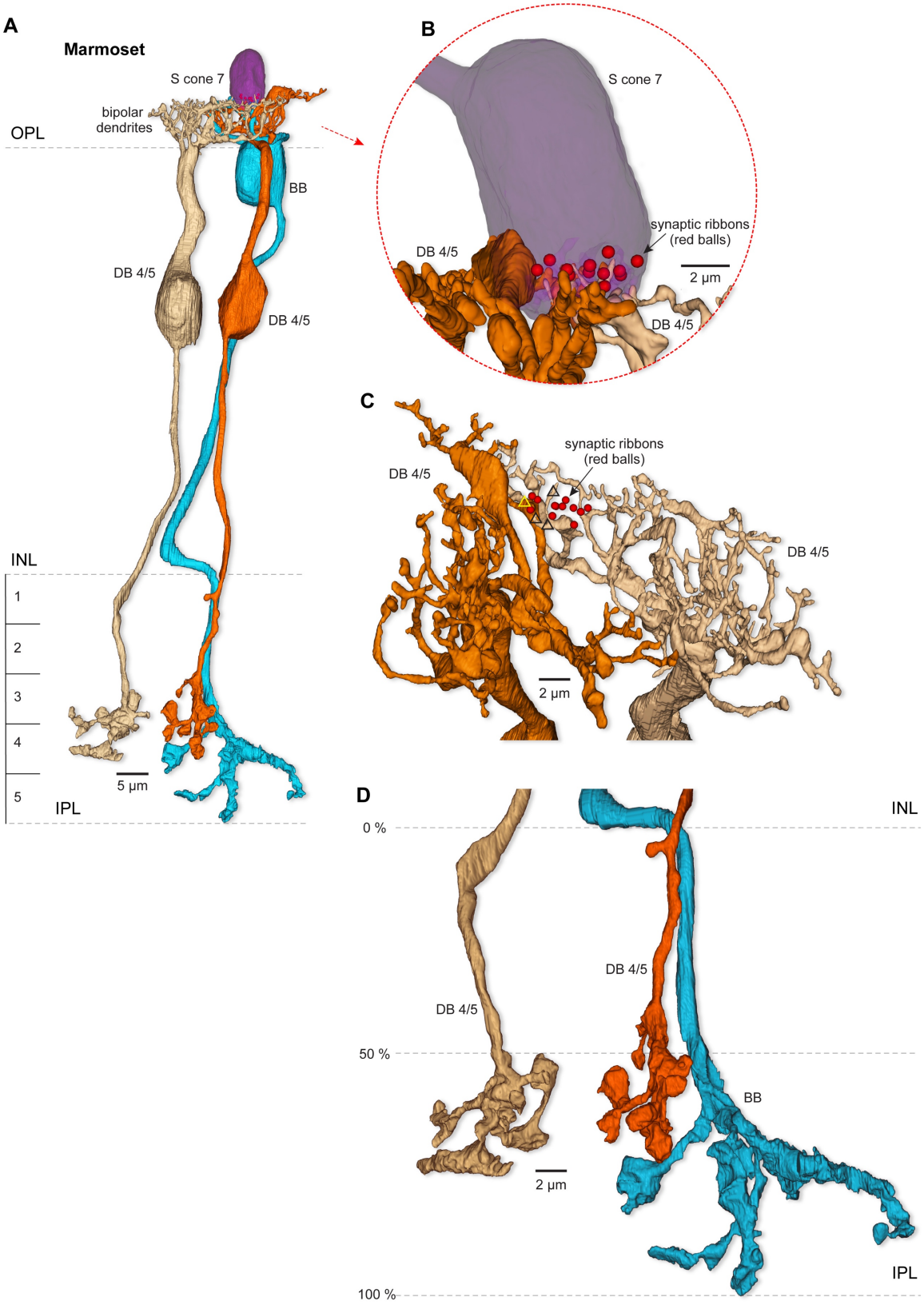
A
Marmoset
S cone 7
bipolar dendrites
OPL
BB
DB 4/5
DB 4/5
INL
1
2
3
4
5
5 µm
IPL
B
S cone 7
synaptic ribbons (red balls)
DB 4/5
2 µm
DB 4/5
C
synaptic ribbons (red balls)
DB 4/5
DB 4/5
2 µm
D
INL
0 %
DB 4/5
DB 4/5
50 %
BB
2 µm
IPL
100 %

Fig. S6. Identification of two presumed ON bipolar cells (DB 4/5) postsynaptic to marmoset S cone 7. A. Vertical image view of two proposed DB 4/5 bipolar cells (tan and orange) postsynaptic to S cone 7, shows both dendritic trees and axon terminals in relation to one of three BB cells targeting this S cone. **B**. Zoomed view of neighboring DB 4/5 cells making flat contacts with S cone 7. **C**. Dendritic trees of the two proposed DB 4/5 cells tile the space around S cone 7 (4 synaptic contacts are indicated by the black and yellow triangles; the cluster of S cone synaptic ribbons are shown as red balls) with little dendritic overlap. **D**. Zoomed view of axon terminal stratification in the IPL; these two neighboring cells showed identical stratification depth in the inner IPL (50-75% depth).

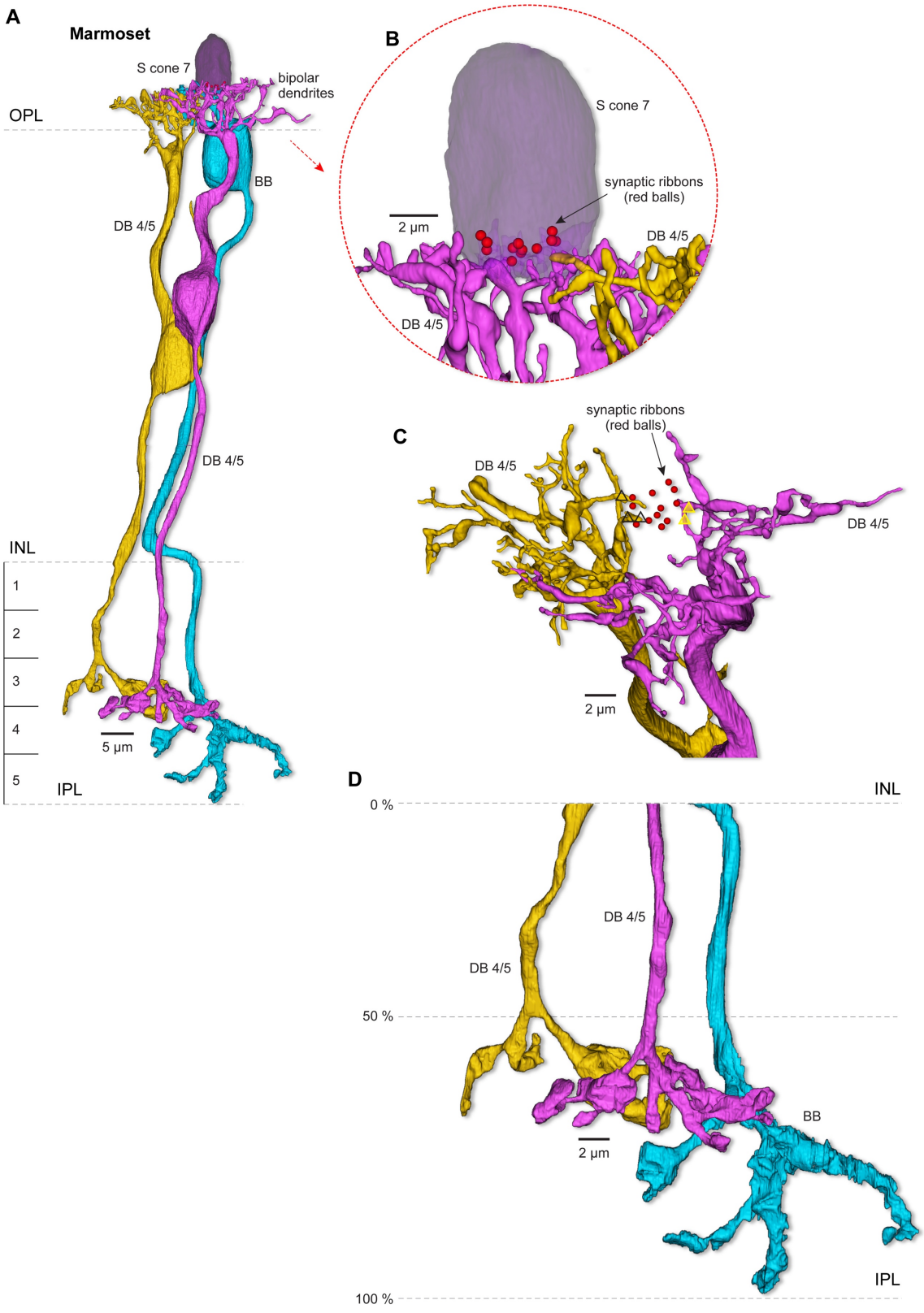

Fig. S7. Identification of two additional DB 4/5 cells postsynaptic to marmoset S cone 7. A. Vertical image view of two proposed DB 4/5 cells (gold and violet) postsynaptic to S cone 7,

shows both dendritic trees and axon terminals in relation to one of three BB cells targeting this S cone. **B**. Zoomed view of neighboring DB 4/5 cells making flat contacts with S cone 7. **C**. Dendritic trees of the two proposed DB 4/5 cells tile the space around S cone 7 (5 synaptic contacts are indicated by the black and yellow triangles the cluster of S cone synaptic ribbons are shown as red balls) with little dendritic overlap. **D**. Zoomed view of axon terminal stratification in the IPL; these two neighboring cells showed identical stratification depth in the inner IPL (50-75% depth).

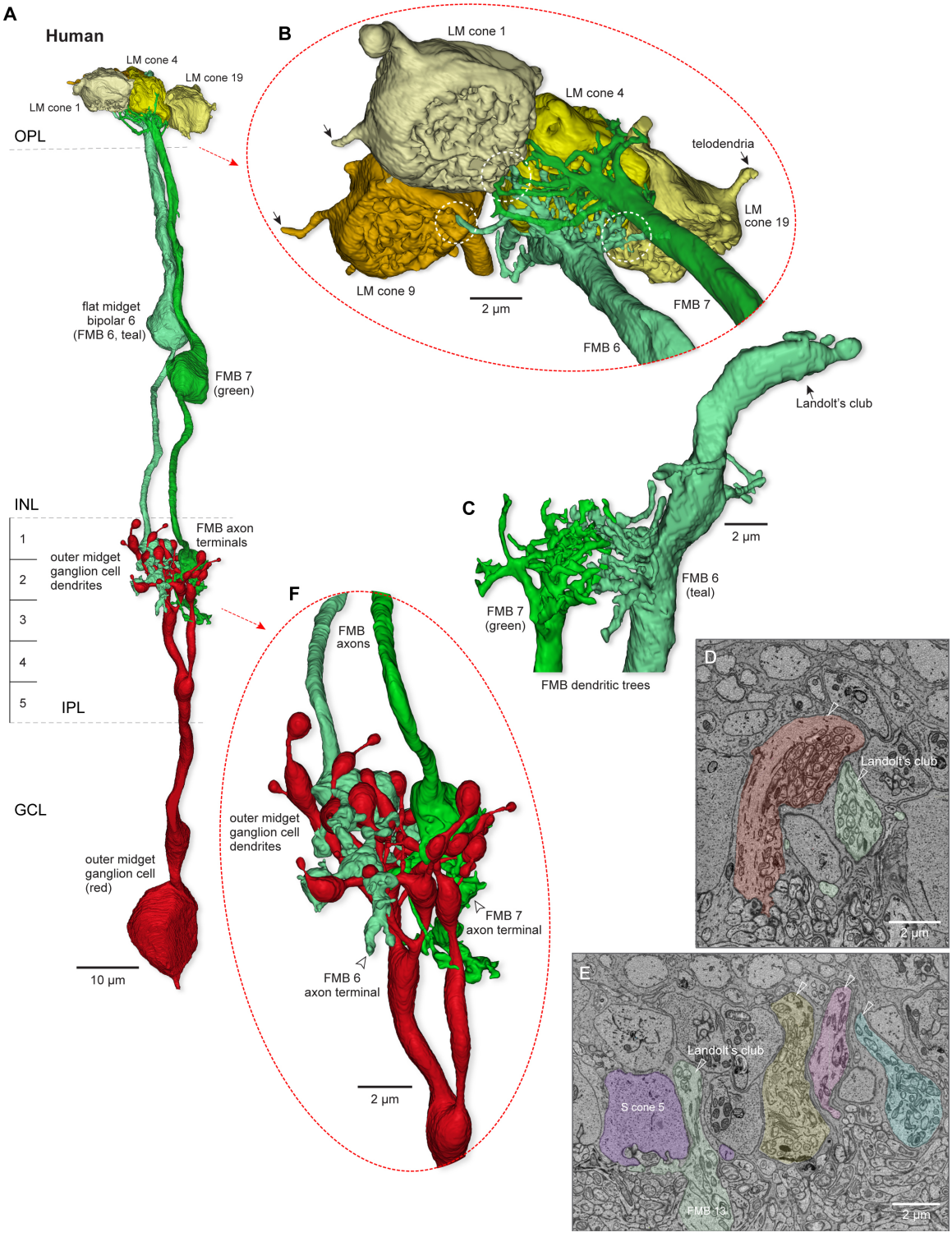

Fig. S8. The human LM cone FMB bipolar circuit. A. Two flat midget bipolar cells (FMB 6; teal and FMB 7; green) target and together carpet the entire synaptic face of a single LM cone pedicle (LM cone 4) and extend fine branches to also sparsely contact three neighboring LM cones (only LM cone 1 and 19 are shown). **B**. Tilted and zoomed view of this connection reveals how these

two midget bipolars share a dense connection with a single cone pedicle of LM cone 4 (yellow) but also send fine branches to contact neighboring pedicles (indicated by the white dotted line circles). **C**. With the cone pedicles removed in this view the dual innervation by two midget bipolar dendritic trees is illustrated in addition to the presence of a distinct Landolt's club on one of the two bipolars similar in morphology to that observed on S cone FMBs like shown in Fig. 6. **D, E**. Landolt's clubs are a distinctive and common feature of the outer human retina (but have not been observed in either the macaque or marmoset retina); they appear to predominantly arise from FMB cells and contain dense networks of mitochondria. The SEM image layers in **D** and **E** illustrate both the Landolt's club for the FMB shown in **C** (teal) in relationship to S cone 5, as well as several other neighboring Landolt's clubs (white open arrowheads, various colors). **F**. Zoomed view of the convergent projection of the two FMBs (teal and green) onto the single dendritic terminal arbor of an outer-OFF midget ganglion (open arrowheads indicates FMB axon terminal arborizations.

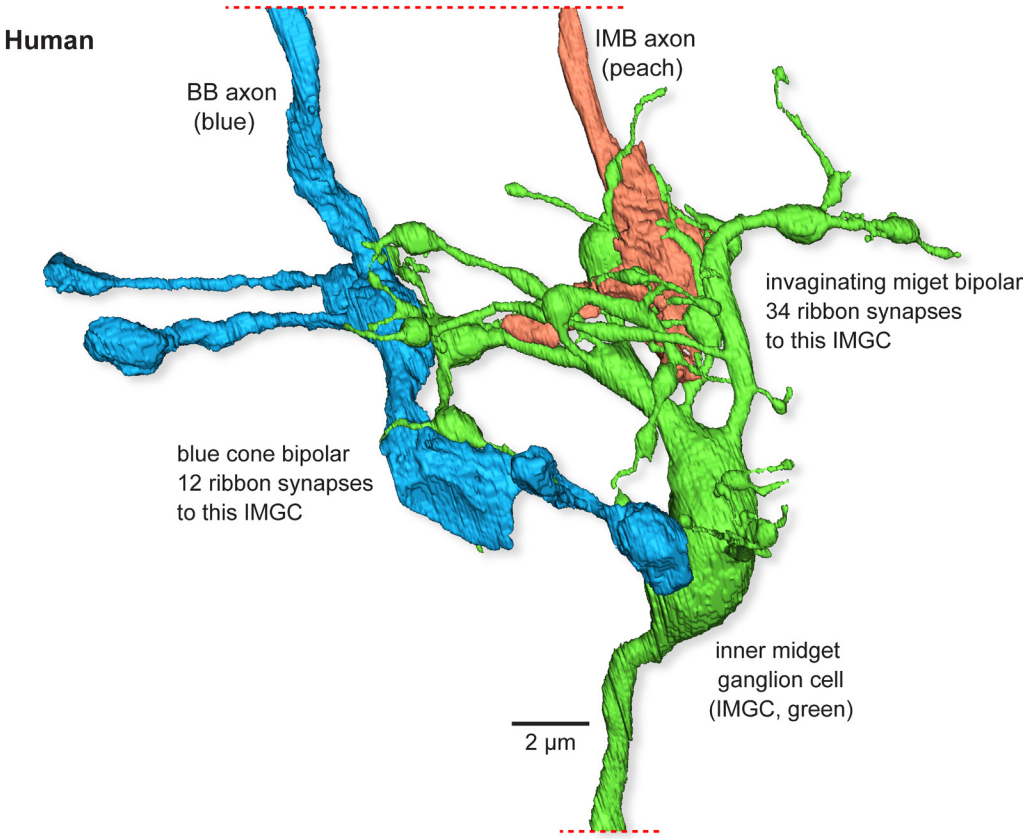

Fig. S9. Human blue cone bipolar (BB) can make extensive synaptic input to inner midget ganglion cells (IMGCs; presumed ON-center type). In human, foveal retina IMGC can receive direct synaptic input from BB cells. BB axon (blue) descends into the inner plexiform layer (IPL) and forms a branched terminal arbor near the IPL inner border. The axon of an invaginated midget bipolar cell (IMB, peach) also enters and terminates deep in the IPL as a single bulbous expansion with little branching. The primary dendrite of the IMGC (green) ascends into the IPL and terminates in a spray of fine branches. The BB axon terminal makes 12 synaptic ribbon contacts with this IMGC and the IMB makes 34 synaptic ribbon contacts with this IMGC. In addition, there were 20 ribbon synaptic contacts not identified as to bipolar origin. Thus at least ~20% of the excitatory input to this IMGC originated from the S cone-BB pathway.

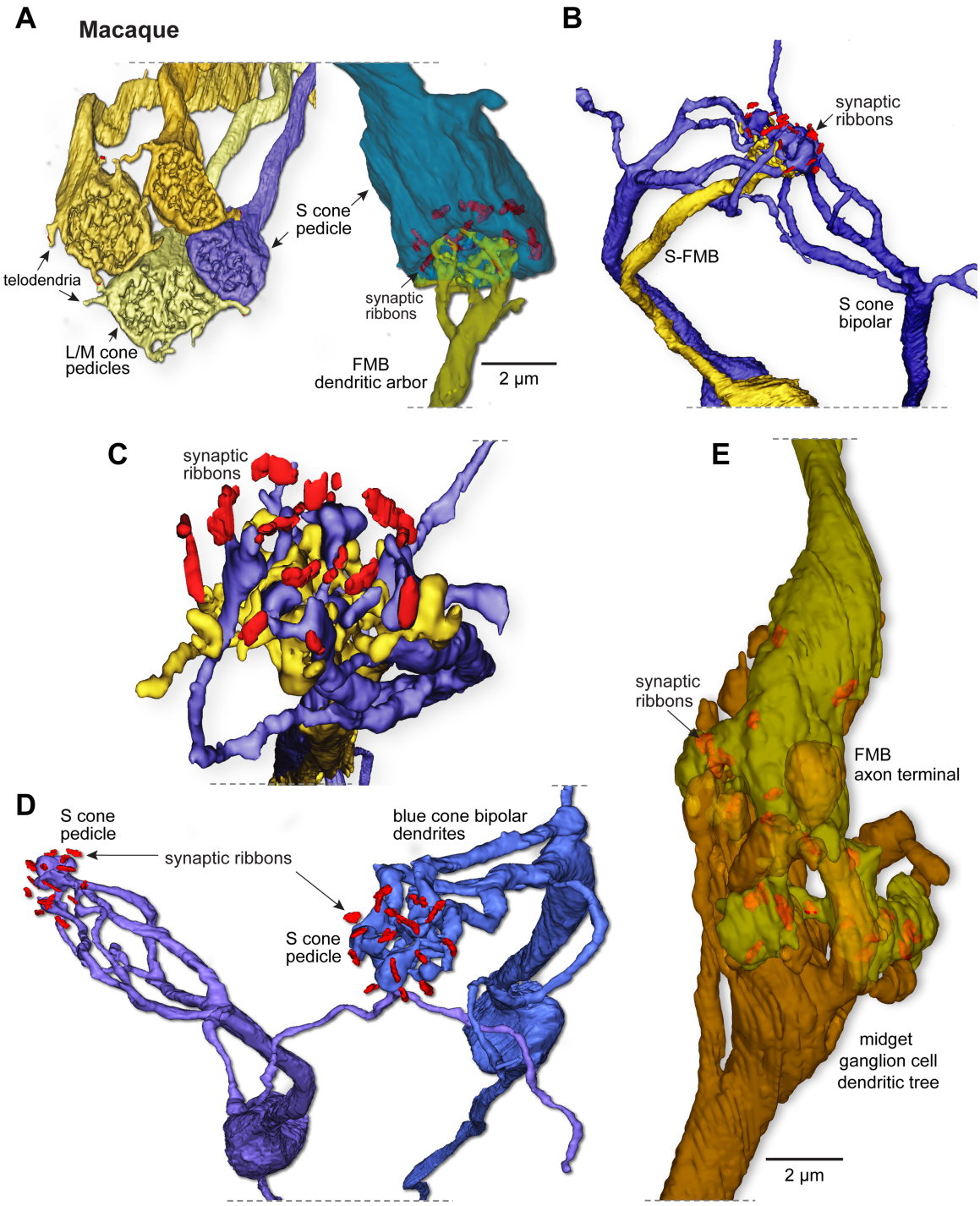

Fig. S10. Cone type-selective connectivity of the S cone circuit in macaque foveal retina (Modified from Wool, et al., 2019, (5)). A. Left, an S cone synaptic pedicle (blue) neighboring 3 LM cone pedicles (yellow/gold). S cone pedicles appeared smaller than LM cones and lacked telodendritic contact with LM cones (see also *SI Appendix*, Fig. 3D for analysis). Right, each S cone (n = 17) made a strictly private line connection with a single flat midget bipolar cell (FMB).

B. Morphology of the blue cone bipolar (BB) type in macaque foveal retina (see also (6)). In addition to a private-line connection with a single FMB (yellow) each S cone receives input from 1-3 BB bipolar cells (blue). All BBs (n = 27) received all synaptic input only from S cones. **C**. Zoomed view of the combined FMB (yellow) basal contacts and BB (blue, invaginating contacts) at a single S cone pedicle. View is looking down at the synaptic face of the pedicle; the pedicle is made transparent and only the synaptic ribbons (red) are shown. **D.** Another view of the selective connectivity of the BB with S cones. Dendrites from one BB extend toward and densely synapse with the pedicle on the left and a second BB extends dendrites to contact the S cone pedicle on the right (pedicles are made transparent and only synaptic ribbons are shown). Each of the two bipolars extend a single dendrite into the outer plexiform layer that ends blindly without contacting a cone pedicle (a common feature of this cell population). **E**. All FMBs made strictly private-line connections with a single outer midget ganglion cell (OMGC, presumed OFF-center type). In this image the FMB axon terminal (yellow) is extending vertically from the top and forms a single globular ending that is enwrapped by the miniature dendritic tree of a single midget ganglion cell (gold) extending vertically from the bottom of the figure.

SI References

1. Zhang C*, et al.* (2020) Circuit Reorganization Shapes the Developing Human Foveal Midget Connectome toward Single-Cone Resolution. *Neuron*, 106(5), 1-14.
2. Kim YJ*, et al.* (2022) Origins of direction selectivity in the primate retina. *Nature communications* 13(1):2862.
3. Drasdo N, Millican CL, Katholi CR, & Curcio CA (2007) The length of Henle fibers in the human retina and a model of ganglion receptive field density in the visual field. *Vision Res* 47(22):2901-2911.
4. Wilder HD, Grünert U, Lee BB, & Martin PR (1996) Topography of ganglion cells and photoreceptors in the retina of a New World monkey: the marmoset Callithrix jacchus. *Visual neuroscience* 13(2):335-352.
5. Wool, L.E., Packer, O.S., Zaidi, Q., and Dacey, D.M. (2019). Connectomic identification and three-dimensional color tuning of S-OFF midget ganglion cells in the primate retina. J Neurosci *39*, 7893-7909. 10.1523/JNEUROSCI.0778-19.2019.
6. Klug, K., Herr, S., Ngo, I.T., Sterling, P., and Schein, S. (2003). Macaque retina contains an S-cone OFF midget pathway. J Neurosci *23*, 9881-9887.